

Apparatus for measuring thermodynamic properties at low temperatures

J. E. Allen, Jr.^{a)}

Astrochemistry Branch, Code 691, NASA Goddard Space Flight Center, Greenbelt, Maryland 20771

R. N. Nelson

Chemistry Department, Georgia Southern University, Statesboro, Georgia 30460

B. C. Harris, Sr.

Machining Technology Branch, Code 547, NASA Goddard Space Flight Center, Greenbelt, Maryland 20771

(Received 11 May 1999; accepted for publication 2 August 1999)

An apparatus has been constructed to provide thermodynamic data for models of planetary atmospheres. Often these data are needed at low temperatures, especially for the outer planets and their satellites, but are not readily available in the literature. The vapor pressure of propane was measured from 85 to 240 K to demonstrate one application of the apparatus for the acquisition of these types of data and to assess the performance of the system. This molecule was chosen because it is available in high purity, it has a well-established vapor-pressure curve, and it exhibits only one phase change over this temperature range. Our results compare favorably with the values available in the literature. The major components of the system include several types of pressure measuring instruments (1000 and 1 Torr capacitance manometers, spinning-rotor gauge), a residual gas analyzer to monitor sample purity *in situ*, and a helium closed-cycle refrigerator for cooling. The gas-handling manifold was constructed using materials and techniques adapted from the semiconductor production industry to minimize sample impurities which constitute a significant source of error in these types of measurements. Several unique design features were also incorporated in the construction of the sample cell to facilitate proper correction for thermal transpiration—an important factor for pressure measurements at low temperatures—and to ensure that the temperature sensor accurately reflected the sample temperature. The operational temperature and pressure limits are 62–240 K and 3×10^{-6} – 10^3 Torr, respectively. The lowest achievable temperature is governed by the no-load temperature of the first stage of the refrigerator and vertical thermal gradients along the sample cell walls, while the minimum obtainable pressure is set by the base pressure of the manifold and a slight outgassing rate. © 1999 American Institute of Physics. [S0034-6748(99)01711-6]

I. INTRODUCTION

The presence of clouds and hazes in the atmospheres of the outer planets and surface frosts on Mars and many of the solid-body satellites have been well established by various ground-based and spacecraft observations. These features are composed of the atmospheric constituents that condense at the cold temperatures prevalent in those environments. Complex descriptive and interpretive models covering a wide range of topics, e.g., surface–atmosphere interactions, condensation of clouds and hazes, and thermal structure, have been constructed to explain these observed features and phenomena. However, reliable results from the models are sensitive to the values for fundamental properties of key constituents or parameters of physical/chemical processes that serve as basic inputs for the models. It is important, therefore, that these data be obtained from laboratory measurements taken under the conditions and over the temperature range pertinent to that object. For the outer planets and their satellites the latter can vary from ~50 to 300 K, but the available laboratory data for some of the most important properties do not cover this range.

Low-temperature thermodynamic data are particularly important for the construction of first-order equilibrium models, but as has been noted,¹ this information for the species of interest is either nonexistent or more likely does not extend to appropriate temperatures. This dearth of low-temperature data is understandable, since the acquisition of thermodynamic data has been driven primarily by industrial needs relating to higher-temperature processes. Thus, most of the available thermodynamic data cover the temperature range from the critical point to the triple point, whereas the planetary community typically requires data below the triple point. In the absence of this information planetary modelers must extrapolate existing higher-temperature data to the temperature range of interest using representations that are not always accurate estimators over large temperature and pressure ranges or estimate the desired quantities on the basis of theoretical arguments.¹ These procedures can lead to errors; therefore, it is important to measure the parameters at temperatures that cover the entire range of interest. The data can then be fitted with various equations to obtain the best representation, thereby ensuring that values are interpolated, not extrapolated, or that extrapolations extend over shorter temperature ranges and are, therefore, more accurate.

^{a)}Electronic mail: john.e.allen@gsfc.nasa.gov

To address the needs of the planetary atmospheres community for this information, we have designed and constructed an apparatus to supply reliable low-temperature vapor-pressure data. Although the principles of vapor-pressure measurements are well developed,² the design, construction, and operation of a low-temperature, low-pressure system presented a number of technological challenges. For example, at the lowest temperatures (~ 50 K) appropriate for the upper atmospheres of the outer planets and their satellites, the vapor pressures of most atmospheric constituents are expected to range from a few Torr to as low as 10^{-7} Torr. (It is customary in the atmospheric sciences to report pressure in units such as millibars or Torr. We adopt that practice here and note that 1 Torr ~ 133.3 Pa.) We chose the static method of vapor-pressure measurements, since it readily lends itself to these types of measurements at low temperatures, and designed the apparatus accordingly. It is well known that there are potentially at least two major sources of error in static low-temperature—and hence, low-pressure—measurements: thermal transpiration and sample purity.² The former results from the fact that the pressure measuring gauge is at a higher temperature than the sample. Sample impurity can arise from contaminants inherent in the original sample, outgassing from the apparatus, or lack of vacuum integrity, i.e., air leakage. Regardless of the source, the effect of impurities on the sample vapor pressure may be more pronounced at lower pressures. Therefore, considerable effort was expended to minimize and/or account for these effects. The effective operating ranges for our system are 62–250 K in temperature and from $\sim 3 \times 10^{-6}$ to 10^3 Torr in pressure. For a given species the pressure or temperature range covered is determined by its vapor pressure and the limitations of our system. Here, we describe the apparatus, measurement procedures, corrections and experimental uncertainties, and the performance of the system with propane (C_3H_8)—a substance with a well-known vapor-pressure curve over our operating ranges.

II. APPARATUS DESCRIPTION

A. Vacuum manifold

As illustrated in the layout in Fig. 1, the vacuum manifold consists of five main sections: high pressure (1000–1 Torr, HP), pressure bridge (bridge), medium pressure ($1-10^{-6}$ Torr, MP), low pressure ($<10^{-5}$ Torr, LP), and residual gas analyzer (RGA) ($\sim 10^{-7}$ Torr). Gas samples are introduced through one of two inlets in the high-pressure section and stored in a detachable sample bulb (SB). The base pressure in this section is monitored by a Pirani gauge (G1) and working pressures, whether during sample transfer or vapor pressure experiments, are measured with a 1000 Torr absolute-pressure capacitance manometer (G2). The “pressure bridge,” represented by the four valves in a rectangular pattern at the center of the manifold, allows the high- and medium-pressure sections to be operated independently; that is, each section can be independently pumped or connected to the sample cell (SC) for either sample transfer or pressure measurements. This bridge also connects the system to the primary vacuum pump stack—comprised of a cold

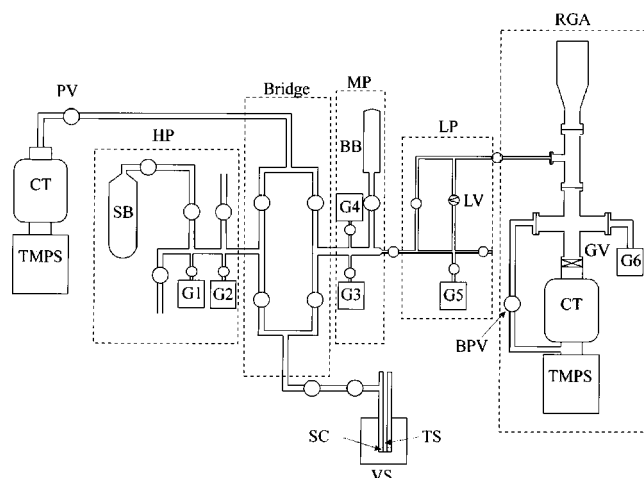


FIG. 1. Overall schematic of the apparatus. The components are grouped by dotted lines into five sections: high-pressure (HP) section consisting of sample bulb (SB), Pirani gauge (G1), and 1000 Torr capacitance manometer (G2); pressure bridge connected to cold trap (CT) and turbomolecular pump station (TMPS) through pneumatic valve (PV) at one end and sample cell (SC) with temperature sensor (TS) and vacuum shroud (VS) at the other; medium pressure (MP) section consisting of ballast bulb (BB), spinning-rotor gauge (G3), and 1 Torr capacitance manometer (G4); low-pressure (LP) section containing leak valve (LV) and cold-cathode gauge (G5); and residual gas analyzer (RGA) section with a separate pump stack, gate valve (GV), and Penning vacuum gauge (G6).

trap (CT) and turbomolecular pump station (TMPS)—through a pneumatic valve (PV) that closes if electrical power is lost, thereby maintaining vacuum integrity. Vacuum plumbing on the TMPS was modified so that the system could be “rough pumped” with the mechanical pump while bypassing the turbomolecular pump. The medium-pressure section contains a ballast bulb (BB) for additional sample storage or transfer in the “clean” side of the manifold and two gauges that are central to the vapor-pressure measurements: a spinning-rotor gauge (G3) and a 1 Torr absolute-pressure capacitance manometer (G4). The inlet of the RGA (Balzers) is connected to the system through the low-pressure section which contains a cold-cathode gauge (G5) to read base pressures and a calibrated leak valve (LV) that can be bypassed through a coarser valve with a higher C_V . This section is used primarily to provide the pressure drop required for best operation of the RGA ($<10^{-5}$ Torr). The RGA section was assembled in a straight line configuration for maximum conductance and is equipped with a dedicated cold trap, turbomolecular pump station, and cold cathode gauge (G6). For mass spectrometric measurements under static conditions the RGA can be isolated from the pump stack by a gate valve (GV). In some cases it is desirable to flow the sample through the RGA to reduce the buildup of dissociation/ionization products. However, with the gate valve fully or even partially open any small samples would quickly be depleted. In addition, it is notoriously difficult to control the throughput of a gate valve; it is essentially binary—either open or closed. Therefore, a bypass valve (BPV) was installed to allow samples to be pumped through the RGA at a much slower rate.

Several steps were taken to ensure vacuum integrity and system cleanliness, eliminate potential outgassing sites or

“virtual leaks,” and maintain sample purity. The system was fabricated using technologies and components adapted from the semiconductor manufacturing industry where, as in our case, the reduction of impurities is of utmost importance. The entire manifold was assembled from 316L stainless-steel parts (tubing, vacuum fittings, valves, sample bulbs) whose interior surfaces are electropolished to reduce adsorption. The high-pressure, medium-pressure, and bridge sections were constructed using tubing with a 1/2 in. outer diameter (o.d.) as a compromise between conductance or pump-down time and the volume of the system; whereas, the low-pressure section was fabricated from 1/4-in.-o.d. tubing to reduce its volume and thereby increase delivery pressure to the RGA. All permanent joints were then butt welded using an orbital welding technique that provides a full penetration weld. This results in a smooth, crevice-free interior, thus eliminating the “virtual leaks” inherent with socket-weld construction. Conflat® flanges and VCR® fittings, both of which seal with metal gaskets, were used for all make-and-break connections throughout the entire system to further enhance vacuum integrity and bakeout capability. The limited use of bellows was deemed important because they present large surface areas and reduce pumping speeds. Hence, only two short (1 in.) stainless-steel metal bellows were incorporated at critical connections to facilitate alignment between components: between the pressure bridge and the manifold pump stack and between the bridge and the sample cell. The line connecting the RGA to its pump stack was assembled from off-the-shelf Conflat® fittings (tee, cross, and full nipple) with an o.d. of 1.5 in. This straight large throat reduces pump-out times and allows the RGA section to reach base pressures in the upper 10^{-8} Torr range.

Except for the capacitance manometers, which are equipped with their own heating units capable of achieving temperatures of ~ 420 K, the complete system is wrapped with heating cables to permit bakeout and further reduce outgassing. The horizontal supports for the manifold are backed with Kapton® insulated flexible heaters and isolated from the main frame of the apparatus by thermal breaks made of phenolic, a low-conductance material. In this way the system can be baked to ~ 350 K, a limit set by the thermal properties of the valve handles. To ensure that the system is evenly heated, yet does not exceed the desired limit, the heating elements of the various sections with their components are powered by separate autotransformers and their temperatures monitored with a series of surface thermistors. Base pressure in the manifold is typically $\sim 10^{-7}$ Torr after baking and pumping with the cryotrap/turbomolecular pump combination. Both the sample bulb and the ballast bulb are wrapped with Kapton® insulated flexible heaters, surrounded by insulating sleeves, and powered by separate autotransformers. They are usually baked at a slightly higher temperature than the manifold to ensure that any residual sample from previous experiments is driven out before a new sample is introduced.

B. Sample cell

Besides concerns about vacuum integrity and system cleanliness, the design of the sample cell was predicated on

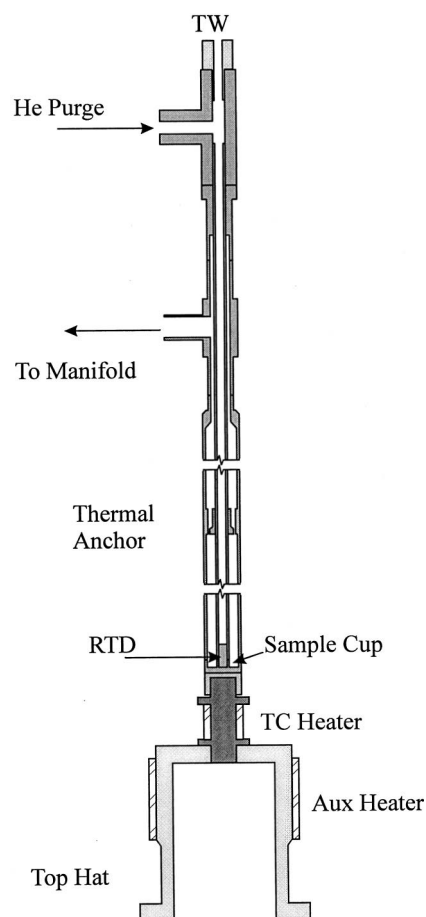


FIG. 2. Cross-sectional view of the sample cell and its thermal connections: (TW) thermal well for temperature sensor probe, (RTD) platinum resistance temperature device, (TC) temperature control heater, (AUX) auxiliary heaters, and top hat bolts to first stage of helium refrigerator.

several additional criteria: The axial and radial temperature gradient should be minimized. The temperature sensor should be as physically close to the sample as possible. The geometry and thermal properties of the sample cell should be well characterized to facilitate pressure corrections for thermal transpiration, an effect that will be discussed subsequently. A cross-sectional view of the sample cell and its related thermal and vacuum connections is depicted in Fig. 2. The same quality materials, components, and techniques were used in assembling the sample cell as were used for the vacuum manifold. Stainless steel (316L) was again chosen for the tubing and fittings because it can be joined by orbital welding and it has a lower thermal conductance than other metals. The latter helps reduce the temperature gradient along the cylindrical axis of the sample cell.

Although the resolution of the drawing is insufficient to show all of the details, the sample cell consists of a set of three nested cylinders equipped with vacuum fittings at one end and capped at the other end by a sample cup. The sample cup itself is shaped like a modified tube pan with a short (0.125-in.-high) outer lip that has an o.d. of 3/4 in. and a taller (0.600 in.) center stub with an o.d. of 1/4 in. The bottom of the sample cup between the inner diameter (i.d.) of the outer lip and the o.d. of the center stub is 0.100 in. thick. The center stub is blind tapped for an 8-32 thread to within

0.100 in. of the backside of the cup; this tapped hole functions as the thermal well for the temperature sensor. A tube 16.05 in. long with an o.d. of 1/4 in. and a wall thickness of 0.035 in. was butt welded to the center stub of the sample cup. The short outer lip of the sample cup was then extended by butt welding to it a tube 5.3 in. long with an o.d. of 3/4 in. and wall thickness of 0.049 in. The top end of this section of the sample cell terminates in a section that thermally clamps it at room temperature. This "thermal anchor" was constructed from a solid piece of stainless-steel bar 1.5 in. long with a 3/4 in. o.d. by boring a 0.652-in.-o.d. hole to a depth of 1/4 in. in each end on axis, then from one end boring a 3/8-in.-o.d. hole to a depth of 7/8 in. as measured from the bottom of the larger hole, and finally, boring the remaining 1/8 in. of material through with a hole that has a diameter of 0.248 in.; this last dimension was critical for assembly. To allow gas to pass through the thermal anchor, six holes with equal angular spacing and 1/8 in. diam were then drilled parallel to the cylindrical axis through the annulus formed between the 3/8 in. hole and the 0.652 in. hole. The extended inner tube (1/4 in. o.d.) of the sample cup was then "cryo-bonded" to the thermal anchor. In this procedure the sample cup with its attached extensions was submerged in a liquid-nitrogen bath until it came to equilibrium at 77 K. This effectively reduced the 1/4 in. o.d. of the sample cup's center-stub extension so that it could be forcefully pressed through the 0.248 in. innermost hole of the thermal anchor until the outer wall of the thermal anchor butted against the 5.3 in. extension of the sample cup's outer lip—these latter two pieces were then joined by orbital welding. On warm up the 1/4 in. inner tube was then automatically bonded to the thermal anchor by mechanically pressing against the undersized hole along the full 1/8 in. contact length. Because both pieces were made from the same type of material, and thus have the same coefficient of thermal expansion, they will remain in contact even when cycled over large temperature ranges. The sample cell was then completed in the following order: A 3/4-to-1/2-in. reducer with a 1/2-in.-o.d. tube extension was butt welded to the top of the thermal anchor; a 1/2-in.-o.d. stainless-steel "tee" that connects the sample cell to the manifold was butt welded to the reducer extension; and a 1/4-in.-i.d. Ultra-Torr® vacuum fitting (reamed to 0.254 in. i.d.) was butt welded to the top of the tee. The extended inner tube (1/4 in. o.d.) of the sample cup passes through the 1/2-in.-o.d. stainless-steel tee and the modified Ultra-Torr® fitting, terminating at the lower end of a 1/4-in.-i.d. Ultra-Torr® tee which is in turn capped with a 1/8-in.-i.d. Ultra-Torr® fitting (reamed to 0.152-in. i.d.). The completed sample cell just slips through a vacuum feedthrough with a 3/4 in. i.d. that is attached to a 6-in.-diam Conflat® flange fixed to the frame of the apparatus. The length of the sample cup's outer lip extension (3/4 in. o.d.; 5.3 in. long) was chosen so that the thermal anchor is surrounded by and in direct contact with this feedthrough when all parts are finally assembled. This ensures that the thermal anchor is held at room temperature. The sample chamber is bounded by the base of the sample cup and at the sides by the 0.652 in. i.d. of the outer tube of the sample cell and the 1/4 in. o.d. of the inner tube of the cell. Thus, the sample is contained in

an annulus that surrounds the thermal well of the sample cup, placing the temperature sensor in close physical proximity. The temperature gradient from the sample cup to the thermal anchor is thereby well established, as is the geometry of the annular cylinder connecting them. Knowledge of these two factors enables us to make a more accurate calculation of the correction for thermal transpiration.

The innermost cylinder, which is not readily visible in the drawing, is removable and houses the primary probe of the sample temperature. It runs the length of the sample cell from the bottom of the sample cup to just above the reamed 1/8 in. Ultra-Torr® fitting at the top, while passing through the 1/4 in. Ultra-Torr® tee. The main length of this probe assembly is a piece of thin-walled (0.010 in.) 304W stainless-steel tubing with a 0.148 in. o.d. that slips inside the inner tube of the sample cell. The tube is open at one end and terminates at the other end in a thermal break made of low-conductance Delrin®. The thermal break is a hollow cylinder 1 in. long with a slight shoulder on one end, so that it press fits into the stainless-steel tube, and 8-32 external threads on the other end to match the internal threads on the center stub of the sample cup. The threads of the thermal break are filed flat on one side to form a "D" shape, and a shallow blind groove, starting at this flat side, runs along the body of the piece. The probe ends at a small cylindrical brass tip that has a center hole blind drilled to within 0.010 in. of the backside of the piece and an o.d. (0.100 in.) that is less than the internally threaded hole (0.162 in. o.d.) of the sample cup. The closed end of the tip is rounded and the other end has a slight shoulder on it to press fit into the threaded end of the thermal break. The tip, thermal break, and stainless-steel tube are attached to one another by small pins made of drill rod filed to the 0.148 in. o.d. of the probe. These pins press fit into holes drilled through these pieces in a direction orthogonal to their cylindrical axis. A Pt resistance temperature device (RTD), traceable to a NIST standard, was coated with a low-temperature thermal grease to enhance thermal contact and then inserted to the bottom of the tip. Because it is not in direct contact with the sample, brass was chosen for the probe tip to increase the thermal conductivity between the sample cup and the RTD.

The design, assembly, and operation of the temperature probe ensures that the RTD only senses the coldest part of the sample cell at the base of the sample cup. Along its lower portion the o.d. of the brass tip is significantly smaller than the i.d. of the sample cup's center stub and the upper portion of the tip is isolated from the stub by the threaded insulating thermal break. Thus, only the very end of the rounded brass tip is in contact with the base of the sample cup when the temperature probe is screwed into the center stub. The thermal break also eliminates any temperature gradient along the stainless-steel tube between the probe tip and the top Ultra-Torr® fitting. As with the RTD, a light coating of low-temperature thermal grease was also applied to the very end of the brass tip before the temperature probe was inserted into the inner tube of the sample cell to further enhance thermal contact. During operation a gas line is connected to the upper 1/4 in. Ultra-Torr® tee and a slow flow of helium passes down the sample cell between the inner wall of the

tube and the outer wall of the temperature probe, then up the inside of the temperature probe via the groove and “D”-shaped threads of the thermal break. This “gas shield” purges air from the temperature probe, eliminating condensation on the probe tip and aiding in the establishment of thermal equilibrium with the sample chamber.

C. Temperature control

Accurate measurement and precise control of the sample temperature are of equal importance to sample purity for reliable vapor-pressure determinations. Both are dependent on good thermal contact between the sample cell and the temperature measuring devices and between the sample cell and the cooling/heating elements. Just as materials were chosen to reduce thermal gradients in the construction of the sample cell, the materials used to connect the sample cell to the temperature measurement and control elements were chosen to enhance thermal conductivity. The use of brass for the tip of the temperature probe, as mentioned above, is an example of this consideration. Thus, the pieces depicted in Fig. 2 that are below the sample cup were fabricated from brass or copper to minimize radial temperature gradients across the sample chamber and maximize axial thermal conductivity along this portion of the system.

To make the transition between the sample cell and the temperature control section, the stainless-steel sample cup was brazed to a brass adapter that is internally threaded. The use of brass for this piece was dictated by two requirements: acceptable thermal conductivity and brazing compatibility with stainless steel. This is a critical joint in the thermal portion of the system and its thermal integrity relies on uniform contact across the faces of the two pieces. To ensure this, a disk of brazing material with a diameter equal to the common o.d. of the sample cup and the adapter was cut from a strip of brazing ribbon, and the joining process completed by uniformly heating this “sandwich” in a high-temperature oven. The internal threads of the adapter mate to the external threads on a brass spool-shaped post, and the height of the adapter is such that it bottoms on the top surface of the post, not the shoulder, as shown in Fig. 2.

The spool-shaped post serves three important functions in the system: It completes the thermal and mechanical contact with the main cooling/heating elements of the system as represented by the “top hat” in Fig. 2. It is the mechanical support for the “temperature-compensation” (TC) heater. And it holds an internally mounted thermocouple that monitors the bottom of the adapter at the joint with the sample cup. Brass was again used as a compromise between thermal conductivity and mechanical considerations. The bottom extension of the post is threaded to match the internal threads in the top hat which is made of copper. Although for thermal reasons copper would be the preferred material for the post, it is more important that the top hat be made of copper, as will be discussed below. Copper-in-copper threads frequently gall, making it difficult to separate pieces, whereas brass-in-copper threads do not exhibit this problem. The center portion of the spool, i.e., between the upper and lower lips, is wrapped with a fine-wire heater that is powered by a

temperature controller and held in place with a circular brass clamp. It is typically operated at power levels from 0 to 2.5 W, which roughly corresponds to a 5 K temperature range for our system. This heater significantly improved the ability to set the temperature of the system by providing fine-temperature adjustment and control. A 3/16-in.-diam blind hole was bored from the bottom of the post to within 1/4 in. of the top. A 0.040-in.-diam hole was then drilled through the center of the remaining 1/4 in. of material. Three small holes spaced 120° apart were tapped (4-40) through the threads at the lower end of the post perpendicular to the cylindrical axis. A fast-response minihypodermic probe with a type-T thermocouple was inserted in the bored hole and held in place by three 4-40 brass set screws that are recessed below the external threads of the post. The thermocouple is implanted in the tip of the 33 gauge (0.008-in.-o.d.), 1-in.-long stainless-steel hypodermic needle. When assembled, the needle passes through the small (0.040-in.-diam) center hole and just makes contact with the inside bottom surface of the adapter and, therefore, the sample cup. This thermocouple monitors the sample temperature from the underside of the sample chamber and is used both as a rough check of the Pt RTD temperature probe embedded in the sample chamber and to assess thermal gradients between the sample cell and the cooling/heating elements.

The “top hat,” so named for its shape, is the center point for temperature adjustment, control, and stability. At the bottom it is bolted to the first stage of a closed-cycle helium refrigerator (cryocooler) that can achieve a nominal base temperature of 45 K with no load. The brass post described above threads into a centered hole tapped through the top of the piece. When the post is tightened down, the lip of the spool makes contact with the top surface of the top hat. Because thermal conductivity is critical at these junctures, the top hat was fabricated from a solid piece of copper stock. This eliminated the need for soldered or brazed joints in construction and ensured that the end surfaces are flat for uniform contact with the cryocooler and the post. The piece is also massive, which reduces thermal resistance and increases thermal stability, although it requires more cooling capacity to reach operating temperatures in a reasonable time. The top hat has an overall height of 5.5 in. with an undercut so that the o.d. is 2.6 in. for the top 3 in. and 2.16 in. for the next 2.25 in. to allow clearance for the screws that attach the 1/4-in.-thick flange at the bottom to the first stage of the cryocooler. A 1.8-in.-diam hole was bored through the center to within 1/2 in. of the top to provide ample clearance for the second stage of the cryocooler. Two slots 1/4 in. wide were machined through the wall along the length of the shorter, narrower bottom section to vent the volume between the interior of the top hat and this stage of the cryocooler. Although the second stage can attain a lower base temperature (10 K with no load), it is not used because its heat dissipation is much slower and the mass or thermal inertia of the system is so large that reaching thermal equilibrium at each desired temperature would make a measurement sequence unrealistically long. Two shallow (0.010-in.-deep) grooves with a width of 1 in. and separated by 1/8 in. were machined around the circumference of the larger top end of

the top hat to confine a pair of auxiliary heaters, as illustrated schematically in Fig. 2. These two Kapton® insulated flexible heaters are 1 in. wide and 8 in. long, so that they just fill the grooves and span the circumference of the top hat. The heaters are held in place by two closely fitting circular brass clamps that also ensure good contact with the top hat. They are controlled by a variable autotransformer and are used for “coarse” temperature control or rapid warm up of the sample cell. Each has a wattage rating of 5 W/in.² and can be connected in series for a maximum power of 20 W, operated individually for a maximum power of 40 W, or in parallel for a maximum power of 80 W. In this way the quadratic dependence of power on supply voltage can be spread over a larger range and the power is more controllable. The combination of these coarse heaters to set the basic temperature level and the fine-wire heater for actual control greatly improved the temperature stability of the system. Three additional thermocouples (type E) are attached to surfaces on the exterior of the sample cell’s brass adapter and at the top and bottom of the top hat to monitor axial temperature gradients between the thermal control elements and the sample chamber.

The minimum temperature currently achievable at the base of the sample cup is 62 K, set by heat leakage along the stainless-steel tubes that connect the sample cup to the thermal anchor. When used together, the heaters are sufficient to raise the temperature to a maximum of 250 K. This operating temperature range covers the condensation points for many constituents of air, e.g., oxygen, argon, water vapor, etc. Therefore, the stack from the thermal anchor to the bottom of the first stage cooler is contained in a 6-in. Conflat® tee that attaches to the 6-in.-diam Conflat® flange at the top and to the cryocooler flange at the bottom via an adapter flange. This shroud is then evacuated to prevent condensation and eliminate heat loss by convection.

D. Pressure measurement

For many substances the operational temperature range of our system corresponds to a range in pressure that covers many orders of magnitude, requiring the use of several gauges. The desirability of measuring these pressures in a single apparatus placed certain constraints on the choice of gauges and their placement in the system. At least one gauge had to have an upper limit above atmospheric pressure both for high-end vapor pressure measurements and as a monitor when transferring the sample into the apparatus. The other gauge(s) had to extend the range to pressures on the order of the base pressure of the system ($\sim 5 \times 10^{-7}$ Torr). To simplify calibration, it is also desirable that the gauges measure pressure directly via a mechanical change rather than through a surrogate such as a change in a thermal conductivity or current. These latter types of gauges—Pirani or ionization gauges, respectively—are calibrated for air and are well suited for the determination of the base pressure of the system. As indicated in Sec. II A above, our manifold and the RGA stack are equipped with Pirani and cold-cathode gauges, but they are only used as base-pressure indicators not to measure vapor pressures. In fact, they are valved out of the manifold during a vapor-pressure experiment to prevent

their contamination by the sample, reduce the total sample volume, and eliminate “ion pumping.” With the above criteria in mind, we chose two capacitance manometers (MKS Baratron®)—one with a 1000 Torr maximum, the other a 1 Torr maximum—and a spinning-rotor gauge (MKS®) as our standard instruments for vapor-pressure measurements. The manifold was designed to be as symmetric as possible, so that the path from the sample cell to each of the three gauges is the same distance with the same number of bends. In this way all three gauges experience the same conditions and monitor the same pressure.

The capacitance manometers are absolute gauges with a specified dynamic range of 10^5 that read pressure by measuring the flexure in a thin metal membrane, and therefore, do not depend on the nature of the gas. To decrease their sensitivity to ambient temperature changes and thereby extend reliable measurements to lower-pressure ranges, they are maintained at a constant 318 K (45 °C) by an internal heat source and thermostat. Their signals are conditioned by a controller with gains of $\times 1$, $\times 10$, and $\times 100$ corresponding to full-scale pressures of (1000, 100, 10) Torr and (1, 0.1, 0.01) Torr for the 1000 Torr and 1 Torr gauge heads, respectively. The readout for each scale has a 10^2 dynamic range, providing an overlap of at least one order of magnitude with which to crosscheck the two heads. For cross-comparison purposes the gauges are usable over most of their specified dynamic range since this procedure takes a short time and can be performed with any gas at room temperature. However, it is our experience that during an experiment, where measurement times are much longer, the effective dynamic range is 10^3 , limited by noise in the output and precision in the readout. In particular, zero on the most sensitive scale of the 1 Torr head drifts too much for long-term measurements, i.e., more than a few minutes. Nonetheless, this scale can be used for short-term checks immediately after a zero setting without rechecking.

Like the capacitance manometers the spinning-rotor gauge (SRG) also measures pressure via a mechanical change. In brief, a steel ball or rotor, contained in a small cylindrical cell, is suspended and spun to a set frequency by an alternating magnetic field. When the alternating field is stopped, the ball decelerates due to drag by the gas in contact with it. The deceleration is correlated with the pressure and after a predetermined time the ball is spun up again to update the measurement. Unlike the capacitance manometers this gauge is not absolute, but is dependent on properties of the gas. In the lower-pressure or molecular-flow regime a knowledge of the atomic weight of the gas is required, whereas in the upper-pressure or viscous-flow regime it is necessary to know the viscosity of the gas. Atomic weights can easily be computed for any molecule; however, viscosities are not as readily available. The specified operating range of the SRG is from ~ 1 to 10^{-7} Torr. However, as was the case with the capacitance manometers and based on our experience with these types of vapor-pressure measurements, the effective operating range is significantly less: $0.1\text{--}3 \times 10^{-6}$ Torr. Above ~ 0.1 Torr, drag decelerates the rotor so rapidly it has to be spun up frequently, leading to heating of the ball that cannot be dissipated before the next update cycle begins.

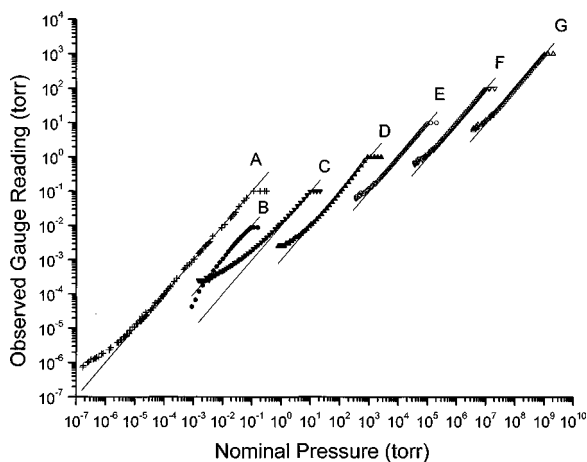


FIG. 3. Comparison of observed gauge reading with nominal pressure: (A) spinning-rotor gauge; 1 Torr capacitance manometer on (B) $\times 0.01$, (C) $\times 0.1$, and (D) $\times 1$ scales; and 1000 Torr capacitance manometer on (E) $\times 0.01$, (F) $\times 0.1$, and (G) $\times 1$ scales.

This makes it difficult to make a meaningful measurement since the response of the ball and surrounding gas change with heat. The practical lower limit is determined by the slow drift and reset produced by residual eddy current drag on the spinning rotor. Each time the ball is spun up, its orientation changes slightly inducing a slight change in the eddy current drag. Under static pressure conditions this imparts a saw-toothed varying offset of about 3×10^{-7} Torr with a period of 5–30 min, depending on the pressure. This difference in specified and effective ranges notwithstanding, there is still an order of magnitude overlap with both the $\times 10$ and $\times 100$ scales of the 1 Torr capacitance manometer. This is convenient because it allows us to set the upper range of the SRG under static conditions by adjusting the viscosity entered in its controller until the displayed pressure matches the reading on the 1 Torr capacitance manometer.

As indicated in the preceding discussion, a key feature of our apparatus is that the ranges of the three pressure gauges overlap so they can be checked against one another. This is clearly illustrated in Fig. 3 where the observed gauge reading is plotted against the nominal pressure. This latter quantity was determined by utilizing the temperature dependence of the vapor pressure of C_3H_8 since it has been well characterized over the temperature range of our system.³ To accomplish this, the manifold was pumped to its base pressure and all of the gauges zeroed. A C_3H_8 sample was then introduced into the system and cryopumped into the sample chamber with the cryocooler. The system was allowed to equilibrate at each temperature setting and readings were taken with the appropriate gauges. These observed values were then compared with the literature value of the vapor pressure of C_3H_8 at that temperature. To avoid overlap and thereby improve clarity, the nominal pressure values of each (gauge \times scale) setting have been successively offset by an order of magnitude for increasing pressures. Thus, the results for the SRG are plotted correctly, whereas the results for the 1000 Torr head on the $\times 1$ scale are shifted to the right and must be multiplied by 10^{-6} to obtain the correct value of nominal pressure. Figure 3 shows the observed gauge readings cov-

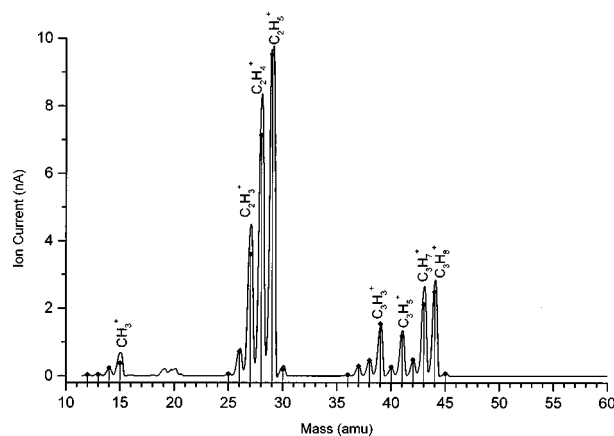


FIG. 4. Mass spectrum of purified C_3H_8 taken *in situ* with the residual gas analyzer.

ering roughly nine orders of magnitude in pressure from 10^{-6} to 10^3 Torr. The flattening of each curve at the upper end reflects the maximum pressure limit of the gauge for that range and the tail off at the lower end is a manifestation of the sensitivity or offset limits of the gauge. The downturn on the lowest scale of the 1 Torr capacitance manometer is the result of zero drift leading to readings less than zero. It is apparent that the capacitance manometers have a usable range of about two orders of magnitude for each scale, while the SRG has a dynamic range of almost five orders of magnitude.

E. Mass analysis

As noted in the introduction, sample purity is one of the largest sources of error in vapor-pressure measurements.² This is particularly true for static methods with a system such as the one described here. To address this problem, a residual gas analyzer was incorporated in the apparatus to check samples on-line, i.e., *in situ*. The RGA is essentially a small mass spectrometer with a mass range of 200 amu that operates at pressures from 10^{-9} to 10^{-5} Torr. Since the RGA is species specific, we can monitor the cleanliness of the system, track the results of sample purification procedures, and verify the purity of the final sample. Typically, the sample purity is checked with the RGA immediately before and after a series of experiments with a particular compound. An example of the mass spectrum for C_3H_8 taken with this instrument is indicated in Fig. 4. This spectrum was obtained with 10 Torr of C_3H_8 in the manifold and a pressure of 5×10^{-5} in the RGA. The points on the graph indicate the positions of ion peaks characteristic of the cracking pattern for C_3H_8 as obtained from a library spectrum provided with the RGA control software.

F. Data acquisition

Real-time monitoring of temperature and pressure is important during bakeout and essential during an experimental run. These activities, e.g., reducing the background in the manifold or establishing thermal equilibrium in the sample at

a new temperature set point, can take long periods of time, so the apparatus was designed to collect readings of the temperature and pressure sensors automatically with a data acquisition system. To realize the full benefit of the RGA, it was necessary to interface its controller to a PC; thus, this controller/PC combination formed the basis for the data acquisition system. A multichannel analog-to-digital (A/D) board was added to the controller and data acquired by the computer under control of data acquisition software supplied with the RGA. The outputs from the temperature controller and controllers for the capacitance manometers, SRG, and cold-cathode gauges are connected to the PC through the A/D board. In this way it is possible to acquire and store values from the following devices simultaneously: the RTD sensor (the sample chamber temperature), one of the thermocouples on the top hat, one of the surface thermistors on the manifold (ambient temperature), one of the capacitance manometers, the SRG, and the cold-cathode gauges. The data can be collected at time intervals ranging from several per second to every few minutes. When the system is being baked and pumped to clean it between experiments, readings are recorded by the data acquisition system at intervals of several minutes over the duration of the heating/cooling cycle. During a typical experimental run the computer is set to store temperature readings from the RTD and the thermistor as well as pressure readings from the appropriate pressure gauge(s) every 20 s. While making vapor-pressure measurements, these data are also recorded at longer period intervals directly from the displays of the various instruments both as a check on the data acquisition system and to link the automatically acquired data to any changes in experimental settings such as heater power or the addition of gas.

III. CORRECTIONS AND UNCERTAINTIES

A. Thermal-transpiration correction

When making low-temperature measurements, the single most important correction to the vapor pressure is for thermal transpiration. This effect is a manifestation of the temperature difference between the sample and the pressure gauge. In our case the sample temperature can range from 250 to as low as 62 K, whereas the SRG is at 298 K and the capacitance manometers are at 318 K. As a consequence the sample chamber can act as a "cryopump," resulting in a gauge reading that is different than the actual pressure. The correction factors for this effect depend on the pressure regime in which the measurements are made.⁴ In the high-pressure limit ($p > 0.75$ Torr) the pressure measured by the gauge will be equal to the sample pressure, i.e., $P_g = P_s$, if the system is in equilibrium and the mean free path of the gas molecule is much less than the diameter of the tube connecting the pressure gauge at T_g to the sample region at T_s . In the low-pressure limit ($p < 7.5 \times 10^{-5}$ Torr) molecular-flow conditions will prevail and thermal transpiration will become important, if the mean free path of the gas is comparable to or greater than the diameter of the connecting tube. Then the pressure gauge will read a higher pressure than the true pressure at the sample cell and the pressure

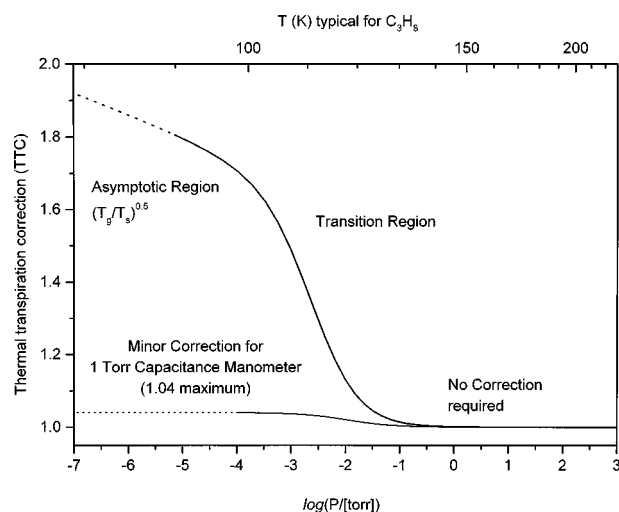


FIG. 5. Thermal transpiration corrections for the sample cell and the minor correction for the 1 Torr capacitance manometer.

ratio will approach Knudsen's value which is the square root of the ratio of the absolute temperatures or $P_g = P_s (T_g / T_s)^{1/2}$. For intermediate pressures it is necessary to calculate this correction using empirical equations that depend on the temperatures of the sample and the gauge, the diameter of the tube connecting them, and the molecular diameter of the gas.⁴ The treatment proposed by Takaishi and Sensui⁵ appears to be the most useful and has been successfully applied to a variety of gases, including C_3H_8 .⁶

Because accurate measurements of low-temperature vapor pressures are critically dependent on properly treating thermal transpiration, particular attention was given to the design of the sample cell, as described in Sec. II B, to facilitate the calculation of the major contribution to the correction for this effect. Recall that the sample cell is constructed of tubes whose diameters are constant from the sample cup to the thermal anchor. The gas is brought to equilibrium at ambient temperature (~ 298 K) at this latter point, thereby establishing a uniform vertical temperature gradient and ensuring the applicability of the Takaishi and Sensui model.⁵ Although the region between the sample cup and the thermal anchor is annular, an equivalent tube diameter can be inferred by considering the possible mean free paths of a gas molecule in this straight cylindrical geometry. In the molecular-flow regime the minimum mean free path will be the width of the annulus, whereas the maximum can be estimated from the maximum path determined geometrically by tangents to the outer wall of the inner tube that intersect the inner wall of the larger tube. The equivalent diameter is then calculated as an average of these two quantities. The effect of thermal transpiration for propane (C_3H_8) in our apparatus is illustrated in the Fig. 5. It is similar in shape to that calculated by others⁴⁻⁶ and can account for factors > 1.8 in our low-pressure measurements for this gas.

Data acquired with either of the capacitance manometers or the SRG must be corrected for thermal transpiration, and the range of pressures covered by a particular gauge determines which formulation of the correction is to be applied. Referring again to the plot in Fig. 3, the lowest pressure (~ 0.2 Torr) at which the 1000 Torr capacitance manometer

can be reliably used is only slightly below the thermal transpiration high-pressure limit. Above this point $P_g = P_s$ and no correction is necessary for most of the measurements made with this gauge. By contrast, except for the extreme upper limit of its pressure range, all of the pressures measured with the 1 Torr capacitance manometer must be corrected for thermal transpiration using the prescription outlined by Takaishi and Sensui⁵ as depicted in Fig. 5. In addition, a similar adjustment must also be made to account for the difference in the thermostatic temperature (318 K) of the gauge and the ambient temperature of the thermal anchor (298 K). By design, once the gas has been equilibrated at the thermal anchor it will remain at 298 K throughout the manifold. Thus, for this correction the diameter of the inlet tube to the capacitance manometer is employed in the Takaishi and Sensui model. As indicated in Fig. 5, the curve generated to account for this temperature difference is significantly lower in magnitude. Compared to the more pronounced correction for the vertical temperature difference of the sample cell, this one is very minor and reaches a maximum of $\sim 4\%$ for the $(T_g/T_s)^{1/2}$ asymptote, i.e., below the thermal-transpiration low-pressure limit. Like the 1 Torr capacitance manometer, most pressures acquired by the SRG can be corrected using the major curve in Fig. 5 since the upper end of the SRG's operating range is below the thermal-transpiration high-pressure limit. The lower end of the SRG's range is below the thermal-transpiration lower-pressure limit, and for measurements in this region the $(T_g/T_s)^{1/2}$ correction should be employed. Unlike the 1 Torr capacitance, no additional minor adjustments are required to the SRG measurements because this gauge operates at 298 K.

B. Outgassing correction

Although our system is quite vacuum tight, a certain amount of outgassing or desorption from the walls is unavoidable. It is typically on the order of $1-3 \times 10^{-8}$ Torr/s and only becomes a problem at pressures below about 1×10^{-4} Torr, where the several minutes required to obtain 5–10 updates of the spinning-rotor gauge can result in a pressure change $\sim 2 \times 10^{-6}$ Torr. Since the data acquisition system can collect data continuously, this capability can be utilized to correct low-pressure measurements for outgassing by following a sequence of steps: First, the sample cell is isolated from the manifold, and the manifold and gauges are pumped to a pressure $< 1 \times 10^{-6}$ Torr. For starting pressures $< 2 \times 10^{-2}$ Torr this only requires a few minutes or less at which time the zero of the 1 Torr capacitance manometer is checked and reset if necessary. This adjustment is particularly important for the most sensitive range ($\times 0.01$), because zero drifts of up to 3×10^{-5} Torr may occur over a 10 min period even though it is held at 318 K thermostatically. To ascertain the base outgassing rate, the manifold is then isolated from the pump and the pressure rise is recorded over a set period of time, e.g., 5 min. The manifold is again evacuated to its base pressure and isolated from the vacuum pump. The valve connecting the sample cell to the manifold is immediately opened, releasing the gas that has been in thermal equilibrium in the sample cell. After an initial jump in pres-

sure due to the introduction of gas to the manifold, the pressure rises linearly and is again monitored for 5 min. Subsequent subtraction of the linear rise for the manifold alone from this measured pressure versus time for the sample results in a constant pressure unless there has been a temperature fluctuation. Note that this correction is not usually needed at higher pressures where the pressure change over a 300 s period (1×10^{-5} Torr or less) is insignificant compared to the measured pressure.

C. Temperature correction

Because the sample cell is cooled at the bottom, a vertical temperature gradient is established from the thermal transpiration station to the sample cup due to conductive heat flow down the walls of the annulus. This temperature variation is roughly linear from a minimum at the bottom of the sample cup to a maximum—ambient temperature—at the base of the thermal anchor, and it can induce a temperature gradient in the sample or between the sample and the sensor. As a result the temperature measured by the sensor may not represent the coldest temperature in the sample; it is the latter that actually determines the vapor pressure. One method by which to assess any required temperature correction utilizes a gas whose vapor-pressure curve is already well known. For sample temperatures above the equilibrium condensation temperature the pressure changes very slowly with temperature (less than 1% per K) in accordance with the ideal gas law. At the point of condensation the vapor pressure can vary by as much as a factor of 10 over a temperature change of 5–10 K, depending on the gas used for the calibration. Hence, when the sample first begins to condense, the pressure will drop precipitously as a consequence of the reduced volume of the condensed phase relative to that of the gas phase. The pressure and temperature sensors can be monitored precisely as a function of time with our data acquisition system and their values at the moment condensation first occurs can be established exactly. The measured pressure at this sharp “break point” corresponds to the vapor pressure of the sample at the coldest point in the sample cell, and a temperature can be related to this pressure via the vapor-pressure curve of the calibration gas which is presumed to be well known. This “vapor-pressure” temperature is then compared to the temperature measured by the Pt RTD. Since the apparatus is a closed system, different “vapor-pressure” temperatures can be determined by changing the starting pressure of the sample in the manifold. Thus, by repeating this process for a series of starting pressures, it is possible to ascertain the uncertainty over a range of temperatures.

Experiments such as those described above were performed for C_3H_8 , a molecule whose vapor-pressure curve is well established, and an example of a determination for one temperature is illustrated in Fig. 6. Here the temporal responses of the capacitance manometer and the temperature sensor have been combined to yield a plot of pressure as a function of the temperature. The triangles represent measurements using an evaporation method, while the inverted triangles correspond to those acquired by the condensation

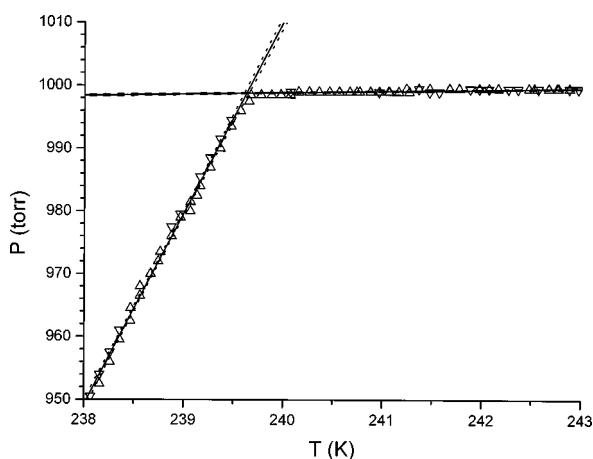


FIG. 6. Evaporation (Δ) and condensation (∇) curves for calibration of the Pt RTD temperature sensor.

method. The solid lines are a best fit to the data obtained by the condensation method and the dotted lines represent 95% confidence limits. The procedure was repeated for several temperature/pressure combinations and the difference between these “vapor-pressure” temperatures and the readings of the Pt RTD was found to be constant over the temperature range. It corresponds to about 3% of the difference between ambient temperature and the Pt RTD reading, so the effect of the temperature gradient is more pronounced at lower temperatures, as would be expected. In order to compensate for this, the sample cell is operated with a nearly constant volume of material in the condensed phase.

Although it is not apparent in Fig. 6 due to the high C_3H_8 pressure at this temperature, for lower temperatures (hence lower pressures), we have generally found the condensation method to be more accurate than the evaporation method, which is consistent with the recommendation that equilibrium between two phases be approached via condensation rather than evaporation.² For our sample cell design this may be attributable to better temperature control, and therefore, a more uniform vertical temperature distribution when the sample cup is being cooled rather than heated. Starting from ambient temperature, the coldest point in the sample cell is assured to be at the base of the sample cup during cool down, and condensation will occur in the vicinity of the Pt RTD. To employ the evaporation method, the sample must first be condensed in the sample cup prior to initiating warm up. At this time the sample cell is in equilibrium with a uniform thermal gradient along its cylindrical axis. When heat is applied to the sample cup, the thermal inertia of the sample cell may result in a cold spot along the cell wall where material evaporating from the sample cup can recondense. Upon further heating this spot will warm, releasing material at a temperature lower than the reading on the sensor in the sample cup.

D. Temperature and pressure uncertainty

Uncertainty in the temperature of the sample directly contributes to the uncertainty in the vapor pressure, and therefore, must be assessed to determine the overall experimental error. As the sample cell is designed here, the Pt RTD

sets the temperature scale for vapor-pressure measurements. This temperature sensor has a specified accuracy of ± 0.25 K and a precision of ± 0.01 K over our operating range (62–250 K). However, our present temperature controller displays the temperature to 0.01 K, but limits data acquisition via computer to a precision of ± 0.1 K.

Uncertainty in the pressure due to the temperature uncertainty varies both with species and with temperature for a given species. The former is related to vapor-pressure specificity, i.e., the vapor pressure developed at a given temperature changes with species. In the latter case the uncertainty in temperature increases as the temperature decreases, as noted above, independent of species. Thus, the uncertainty in pressure would also be expected to vary with temperature in a similar fashion. For static measurements the pressure uncertainty for various temperatures can be determined from the temperature uncertainty by applying the ideal gas law. For propane, the relative uncertainty in pressure due to the uncertainty in temperature was found to vary from 4% at 100 K to 0.4% at 240 K.

Besides the uncertainty in the temperature, there are a number of other sources that contribute to the overall uncertainty in the pressure measured by our system. These are related to the uncertainties inherent in the gauges themselves and are usually stated by the manufacturer as a percent of either full scale or the actual reading. For the capacitance manometers these include a variety of factors—nonlinearity, hysteresis, nonrepeatability, resolution, internal temperature changes—that are combined to yield a specified total uncertainty, expressed as a percent of reading, of $\sim 0.08\%$. However, it is our experience that the effective total uncertainty is $\sim 1\%$ of the reading over a dynamic range of 10^3 and greater over an additional decade. As indicated in Sec. IID, this is set primarily by noise in the output and precision in the readout and accounts for the deviations from linearity clearly evident at the lower end of the curves in Fig. 3. (Note: The plateau at the higher pressures represents the maximum response for each gauge/scale combination.) Consequently, pressure measurements are made with the capacitance manometers only over the linear portion of each gauge/scale setting, guaranteeing that the effective total uncertainty is $\sim 1\%$. The specified uncertainty in measurements with the SRG depends on the pressures at which the instrument is used. For pressures greater than $\sim 10^{-2}$ Torr the uncertainty varies from 1% to as much as 10% of the reading, whereas for pressures less than $\sim 10^{-2}$ Torr the uncertainty is 1% of the reading plus or minus the variation in the residual drag ($\pm 3 \times 10^{-8}$ Torr). As noted in Sec. IID and illustrated by the linear portion of the curve in Fig. 3, we have found the useful range to be 3×10^{-6} to 0.1 Torr with an uncertainty of 1%–3%. The lower-pressure limit represented by the deviation from linearity is set by periodic changes in the “offset” due to magnetic drag.

The overall uncertainty in pressure was determined by quadratic combination of the uncertainty due to temperature and the appropriate gauge uncertainty. Since the temperature uncertainty increases with increasing temperature difference between the sample cup and the thermal anchor, its contribution is greater at lower temperatures. By contrast the

gauge uncertainties are relatively constant for the pressure ranges over which the instruments are used. Therefore, their contribution to the overall uncertainty is greater at higher temperatures or equivalently higher pressures. For C_3H_8 this results in an overall uncertainty in pressure varying from 4.1% at 100 K to 1.1% at 240 K.

IV. PERFORMANCE ASSESSMENT

The performance of the apparatus and validity of the treatment for corrections can best be evaluated by measuring the temperature dependence of the vapor pressure of a gas for which well-determined values are available in the literature. This at once establishes the system's accuracy and precision for monitoring both pressure and temperature. The choice of such a calibration gas is constrained by several factors: The gas should be available in high purity. The vapor-pressure curve should vary monotonically with temperature, i.e., only one condensed phase of the sample should exist over the appropriate temperature range (62–250 K for our system). The vapor pressure should cover as much of the measurable pressure range as possible (3×10^{-6} – 10^3 Torr for our system). As indicated previously, C_3H_8 is well suited as a calibration source over the operational limits of our apparatus. It is available in high purity (99.95% or better) and its vapor pressure for the gas-to-liquid phase transition spans a pressure range from 10^{-6} to 10^3 Torr for temperatures from 85 to 240 K, respectively.³ Thus, its vapor pressure covers our measurable pressure range and most of our operational temperature range in one phase transition. This molecule is also interesting because it is important in some planetary atmospheres where it is a product of CH_4 photochemistry, formed by the photolysis of ethane (C_2H_6) and subsequent CH_3 reactions.¹ For example, it has been detected in the Jovian atmosphere by infrared spectroscopy⁷ and from the mass spectra of the Galileo probe.⁸

To test our apparatus, the vapor-pressure curve for C_3H_8 was measured over the temperature range from 85 K (the freezing point) to 240 K. Prior to filling the manifold with the C_3H_8 sample, the system was baked for 72 h during which time a sequence of operations were performed to aid in clean up: First, the system was pumped until a minimum pressure was reached; then, it was backfilled to 760 Torr with high-purity nitrogen (N_2) and maintained at this pressure for several hours while baking continued; finally, it was evacuated again until a lower minimum pressure was reached. Because N_2 is nonpolar, heating with a high pressure of N_2 in the system helped to collisionally liberate adsorbed material from the walls. This sequence was repeated several times during the 72 h period until the minimum pressure no longer changed. At this point the system was allowed to cool to ambient temperature while being pumped. To preserve cleanliness during gas transfer, the rest of the manifold was isolated from the high-pressure section via the pressure bridge. Before introducing scientific-grade C_3H_8 (MG Industries, 99.95% minimum purity) into the manifold, the inlet tube from the gas cylinder was pumped back to the shutoff valve on the regulator. The inlet tube was purged several times with C_3H_8 to sweep out or dilute any impurities in this

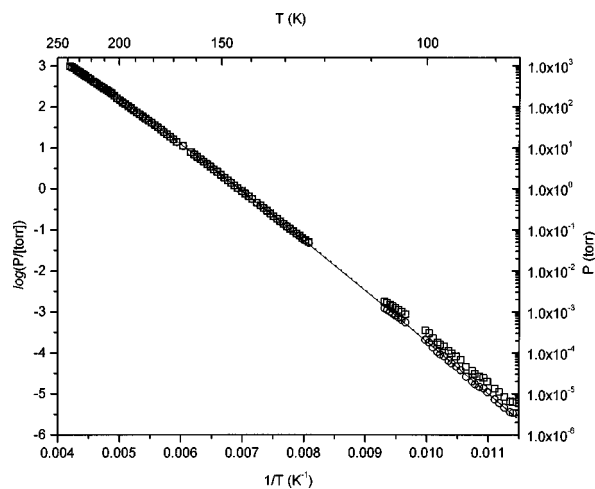


FIG. 7. Vapor-pressure curve for C_3H_8 : raw data (\square), data corrected for thermal transpiration (\circ), literature data (dotted line), and fit to our data with three-parameter representation (solid line).

connection. The system with the gas cylinder attached was then pumped to the lowest achievable pressure. At this juncture the high-pressure section and the sample bulb were filled with several hundred Torr of C_3H_8 . The sample bulb was isolated from the manifold to serve as a gas reservoir, and the sample in the high-pressure section was condensed in the sample cup by the cryocooler. The valve from the manifold to the sample cell was then closed, while the sample in the sample cup was held at cryogenic temperatures. With the gas cylinder isolated from the manifold, the high-pressure section was repressurized by gas from the sample bulb and its contents condensed into the sample cup. This process was repeated until enough sample had been collected to ensure there would be nearly a constant volume of material in the liquid phase. The sample was then subjected to several freeze–pump–thaw cycles to reduce impurity levels further and a small portion was expanded into the RGA for analysis. At this point the sample was recondensed and the system, excluding the sample cell, was pumped to its lowest pressure. The vapor-pressure curve was then mapped by varying the temperature of the sample and measuring the pressure with the appropriate gauge.

Our vapor-pressure data for C_3H_8 are presented in Fig. 7 and, as expected, the effect of thermal transpiration is most noticeable at lower temperatures—compare the raw data (squares) to the corrected data (circles). Each point on the graph generally represents 3–6 overlapping measurements taken over a temperature interval of about 0.2 K within a time span of 3–5 min. A fit to the available literature data,³ depicted as the dotted line most apparent in the region between sets of data points, is also included for comparison purposes. Both the literature data and our data cover a similar range of temperatures, i.e., down to the triple point at 85.5 K.

A number of semiempirical equations can be used to fit vapor-pressure versus temperature data from a simple two-parameter Clausius–Clapeyron equation, corresponding to the first two terms in Eq. (1), to a more complicated five-parameter equation,

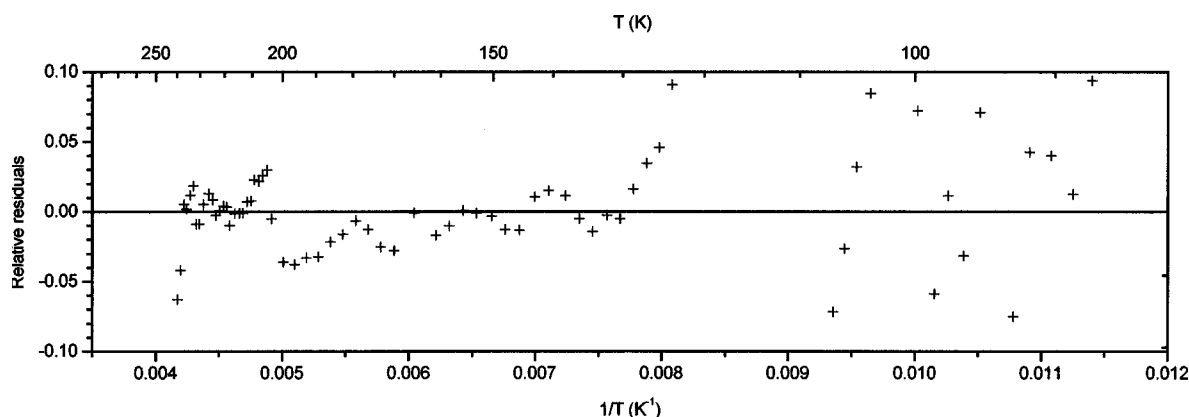


FIG. 8. Relative residuals between our data and the three-parameter fit.

$$\log P = A - (B/T) - C \log T + DT + ET^2, \quad (1)$$

where P is the pressure in Torr and T is temperature in degrees kelvin. The “2.5, 5” form of Wagner’s equation has also been successfully applied to propane data from 94 to 368 K.⁹ This equation, for which pressure and temperature are expressed in reduced form relative to their critical values, appears to be most useful for the portion of a vapor-pressure curve between the triple point and the critical point. In general, more parameters lead to a better fit or allow fitting over a wider temperature range, but the utility of adding terms is limited. For the data presented here we have found a truncated five-parameter equation, i.e.,

$$\log P = A - (B/T) - C \log T, \quad (2)$$

to be an adequate representation. The solid line in Fig. 7 is a fit to our data using this three-parameter equation with $A = 11.877$, $B = 1253$, and $C = 1.521$. A plot of the relative residuals, defined as $[(P_{\text{obs}} - P_{\text{fit}})/P_{\text{fit}}]$, is presented in Fig. 8. Obviously this equation does not fit the data as well at lower temperatures as it does at higher temperatures; however, across the temperature range the relative residuals are on the order of the maximum experimental error. While more complicated expressions may fit slightly better, this comes at the sacrifice of simplicity and ease of use of the representative equation. This latter consideration is not an important issue for thermodynamicists, but may be for planetary scientists who must make approximations in their models that contribute larger errors than these.

V. DISCUSSION

The apparatus described here was specifically constructed to acquire low-temperature vapor-pressure data for species of interest to the planetary atmospheres community. Because conditions in planetary environments vary widely, the system was designed to cover as large a range of temperature and pressure as possible—62–240 K and 3×10^{-6} – 10^3 Torr, respectively. However, for a given species the lower operational limits may not be achieved simultaneously, rather the lower limit of one parameter may set the lower limit of the other. For example, if at our lowest temperature the vapor pressure of the species is lower than our lowest measurable pressure, then the temperature range is set by our pressure measuring capability. Conversely, if the spe-

cies has a measurable vapor pressure at our lowest temperature, then the pressure range is set by our lowest achievable temperature. Several unique features were incorporated to aid in correcting for thermal transpiration which becomes important at lower temperatures and, hence, lower pressures. Overlap of the ranges of the pressure measuring gauges and the ability to monitor sample purity online with the RGA are also important features of the apparatus. The former ensures that the SRG can be calibrated even if the viscosity of the sample is not well known. The operational pressure limit of the RGA overlaps the range of the SRG by two orders of magnitude; thus, these two instruments could be cross calibrated, thereby significantly extending the pressure measuring range of the system if necessary. More importantly the RGA is species sensitive and can, therefore, be used to follow the evolution of substances with temperature. This is a critical feature for the determination of the thermodynamic properties of binary and tertiary mixtures, e.g., fugacities, and we plan to take advantage of this capability. The good agreement of our measurements for C_3H_8 with those available in the literature over an equivalent temperature range suggests that our apparatus is quite adequate for the low-temperature vapor-pressure measurements for which it was designed.

ACKNOWLEDGMENTS

The authors thank F. J. Bloom for his assistance in the design of the manifold and instruction in orbital welding techniques. The authors also gratefully acknowledge support by NASA’s Planetary Atmospheres Program.

- ¹S. K. Atreya, *Atmospheres and Ionospheres of the Outer Planets and Their Satellites* (Springer, New York, 1986).
- ²D. Ambrose, in *Experimental Thermodynamics*, edited by B. Le Neindre and B. Vodar (Butterworths, London, 1975), Vol. II.
- ³V. V. Seychev, A. A. Vasserman, A. D. Kozlov, and V. A. Tsymarny, *The Thermodynamic Properties of Propane* (Hemisphere, New York, 1991), and references therein.
- ⁴K. F. Poulter, M.-J. Rodgers, P. J. Nash, T. J. Thompson, and M. P. Perkin, *Vacuum* **33**, 311 (1983).
- ⁵T. Takaishi and Y. Sensui, *Trans. Faraday Soc.* **59**, 2503 (1963).
- ⁶I. Yasumoto, *J. Phys. Chem.* **84**, 589 (1980).
- ⁷S. J. Kim, J. Caldwell, A. R. Rivolo, R. Wagener, and G. S. Orton, *Icarus* **64**, 233 (1985).
- ⁸H. B. Niemann *et al.*, *Science* **272**, 846 (1996).
- ⁹H. Kratzke, *J. Chem. Thermodyn.* **12**, 305 (1980).